




Enhancement of optical absorption and dispersion characteristics of nanocrystalline In_2Se_3 films: impact of γ -ray irradiation

Bassant Ebraheem^{1,*} , A. A. M. Farag¹, A. H. Ashour², N. Roushdy³, and M. M. El-Nahass¹

¹Thin-Film Laboratory, Physics Department, Faculty of Education, Ain Shams University, Roxy, Cairo 11757, Egypt

²National Center for Radiation Research and Technology (NCRRT), Nasr City, Cairo, Egypt

³Electronic Materials Department, Advanced Technology and New Material Institute, City for Scientific Research and Technological Applications, New Borg El Arab City, Alexandria 21934, Egypt

Received: 22 October 2022

Accepted: 25 December 2022

Published online:

4 February 2023

© The Author(s) 2023

ABSTRACT

Thermal evaporation was used to deposit In_2Se_3 thin films with a thickness of 276 nm on different glass and quartz substrates under vacuum. The ^{60}Co rays were used to irradiate thin films at dosages of 10, 20, 30, 40, and 50) kGy. X-ray Diffraction (XRD) and scanning electron microscopy (SEM) were used to investigate the crystalline and morphological structure of In_2Se_3 thin films, respectively. The results revealed that powder has a polycrystalline structure, whereas pristine and irradiated thin films are amorphous. The computed absorption coefficient indicates that direct transition is allowed for the as-deposited and γ -irradiated thin films, and the value of the measured energy gaps increases when the dose is increased from 10 to 50 kGy. Using single-oscillator models to obtain the dispersion parameters, the spectral dependency of the refractive index in the higher wavelength area was studied. The effect of irradiation on dielectric constants and dispersion characteristics suggests that the examined films are highly sensitive to appropriate irradiation dose. The non-linear optical susceptibility has improved, making it appropriate for a variety of device applications.

1 Introduction

The III–VI semiconductors have caused a great deal of study owing to the unique electrical and optical properties and potential applications in electronic and optoelectronic devices such as phase-change

random access memory (PRAMs), solid-state batteries, and solar cells [1–3]. Some studies involved the fabrication of In_2Se_3 as an optoelectronic material and/or a memory material compatible with complementary metal–oxide semiconductor (CMOS) technology which are taken into account. Then the

Address correspondence to E-mail: bassant.elsayed@edu.asu.edu.eg

perfectly deposited state In_2Se_3 layer can be placed inside the carved slot. The lens can be shifted between the s -state and the p -state via thermal annealing, electrical current injection, and optical excitations [4].

In_2Se_3 is a defective tetrahedral bonding configuration with one-third of the sites unfilled, forming a screw array along the c axis. Because In_2Se_3 has so many distinct crystalline phases, growing high-quality In_2Se_3 with a single phase is challenging. High-quality thin films of In_2Se_3 epilayers were prepared using thermal evaporation approach [5, 6], Bridgman–Stockbarger Method [7, 8], and metal-organic chemical vapor deposition (MOCVD) [9–11]. Environmentally friendly III–VI semiconductor thin films with specified characteristics are required for modern technological applications. III–VI semiconductor thin films are made using chemical or physical processes. One of the most precise procedures in the manufacturing of these films is thermal evaporation under vacuum.

Due to their direct band gap features, which show a higher photon emission and absorption efficiency compared to indirect semiconductors, group III–V materials are generally ideal for optoelectronic devices in light-emitting/absorbing devices, such as LEDs, lasers, and detectors. Thus, Si-based III–V devices and III–V photoelectric devices can significantly increase the data transmission speed and amount by taking advantage of the superior features of III–V compounds, which substantially reduces integrated electricity and power consumption [10]. The III–VI semiconductor materials, including indium selenide (In_2Se_3), have drawn a lot of interest for use in solar cells. In_2Se_3 can be utilized as a window material or buffer layer for solar devices since it has the best physical features. It is an n -type semiconductor that can be successfully deposited using soft methods, and its band gap can change depending on the composition, ranging from 2.0 to 2.45 eV. Most based cells may use thin films of In_2Se_3 as a window material [11].

The effect of irradiation on III–VI semiconductor thin films, on the other hand, has piqued curiosity. The effect of radiation on nanomaterials can help with appropriate design of material characteristics for a variety of prospective applications. Radiation has the potential to change the characteristics of a substance in a single step. Radiation can produce new or different defect states to form as well as changes in trapped charge at defect sites, carrier densities, and

increased oxidation of thin films [10, 11]. When employing electronic equipment in high-dependability applications in severe environments, this irradiation can also assist forecast reliability [12]. The effect of irradiation on inorganic semiconductor thin films in regard of modifying their physical characteristics has been widely investigated and analyzed. However, a technical issue in the optical properties of the In_2Se_3 thin films is still needs further investigations to be able to improve their optical properties of the compound, and the full coverage has not been completed by further authors. Thus, the present study concerns easily prepared method for preparing thin films, unique optical parameters, and adaptable optoelectronic features of the In_2Se_3 films enabled them to be one of the key alternatives compared to the well-known silicon-based traditional solar cells.

The focus of this research is to see how gamma irradiation affects the structural and optical features of In_2Se_3 thin films before and after they have been exposed to dosages of (10, 20, 30, 40, and 50) kGy. There is no extensive examination of the influence of gamma irradiation on the described behavior of In_2Se_3 films made by the thermal evaporation process that we are aware of in the literature. As a result, a thorough investigation of the structural and optical features of In_2Se_3 thin films is necessary. In this paper, a high-quality In_2Se_3 thin film was created utilizing a thermal evaporation approach in a high-vacuum environment to investigate the film's structural and optical features in considerable depth. The XRD and SEM were used to evaluate the film's key microstructural properties. The spectrophotometric approach was used to investigate optical absorption and transitions in the UV–Vis region for In_2Se_3 thin films under the influence of various irradiations. The dispersion of refractive index was also analyzed and described using a single-oscillator model over a broad wavelength range, and the nonlinear optical characteristics were also investigated.

2 Experimental techniques

2.1 Thin-film preparation and characterization of In_2Se_3

The Leybold Heraeus GmbH organization provided In_2Se_3 with a purity of 99.999 percent (5 N), which

was utilized without additional purification. Using a typical thermal evaporation technique, type Edwards Co. model E 306A, England, on completely clean glass and quartz substrates, In₂Se₃ thin films were deposited. Using a thickness monitor made of quartz crystal, the thickness of the prepared films was investigated. A quartz crucible heated by a tungsten coil was used to evaporate In₂Se₃.

The microstructures of material powder and thin films were investigated using a SHIMADZU X-ray diffractometer with CuK_α radiation = 1.540 and operating at 30 mA and 40 kV. The morphology and the crystalline structure of powder and thin films of In₂Se₃ were investigated using SEM and XRD, respectively.

In a ⁶⁰Co irradiator chamber, the thin films were bombarded with γ-rays (Indian cell GC 4000). A concentric source permanently wrapped in a lead shield and a cylindrical drawer that slides up and down along the center axis make up the irradiated unit. A compartment in the drawer holds the samples to be irradiated at a dosage rate of 0.96 kGy/h. To avoid the heat generated by irradiation, a cooling system was added to the cell.

The transmittance, *T*(λ), and reflectance, *R*(λ), of In₂Se₃ thin films at normal incidence in the wavelength range 200–2500 nm were measured using a double-beam spectrophotometer (JASCO model V-670 UV-Vis-NIR) with 10 nm intervals.

2.2 Optical calculation procedure

The absolute values of *T*(λ) and *R*(λ) can be computed by correcting the absorbance and reflectance of the Quartz substrate, which is provided by the following formulae [13]:

$$T = \left(\frac{I_{ft}}{I_q}\right)(1 - R_q), \tag{1}$$

where *I_{ft}* and *I_g* are the intensities of light passing through the film-quartz system and that passing through the reference quartz, respectively. *R_q* is the reflectance of the quartz substrate and

$$R = \left(\frac{I_{ft}}{I_m}\right)R_m(1 + [1 - R_g]^2) - T^2R_g, \tag{2}$$

where *I_m* is the intensity of light reflected from the reference mirror, *I_{fr}* is the intensity of light reflected from the sample, and *R_m* is the mirror reflectance.

The values of the absorption coefficient, α, and optical constants (*n* and *k*) were estimated using the following relationships [14, 15]:

$$\alpha = \left(\frac{1}{d}\right) \ln \left[\left(\frac{(1 - R)^2}{2T}\right) + \left(\left(\frac{(1 - R)^4}{4T^2}\right) + R^2\right)^{1/2} \right] \tag{3}$$

$$K = \frac{\alpha\lambda}{4\pi} \tag{4}$$

$$n = \left(\frac{4R}{(1 - R)^2} - K^2\right)^{1/2} + \left(\frac{1 + R}{1 - R}\right), \tag{5}$$

where *d* represents the film thickness, *T* represents the measured transmittance, and *R* represents the measured reflectance. The computational technique [16] is used to estimate the experimental errors. *R* and *T* computations were determined to be 0.1%, film thickness measurement to be 2.2%, refractive index to be 3%, and extinction coefficient to be 2.5%.

3 Results and discussion

3.1 Structural and morphological investigations

The XRD pattern of In₂Se₃ in powder form is shown in Fig. 1(a). According to Shirly et al.[17], Miller indices for each diffraction peak in XRD were calculated on the pattern using the Crysfire Program. As shown in the picture, a polycrystalline nature with varied preferred orientations was discovered. The XRD patterns of the In₂Se₃ thin film, as shown in Fig. 1(b), are amorphous, with no evident preferred orientations.

Figure 2(b) shows the effect of γ-irradiation with varied dosages of 10, 20, 30, 40, and 50 kGy on the XRD of In₂Se₃ film. The diffraction hump is observed for all films, and this is followed by an increase in full width at half maximum, as well as a modest shift in the hump toward higher 2θ values. This implies that the structural characteristics of the films changed because of the γ-irradiation treatment.

The surface morphology of In₂Se₃ films before and after 40 kGy γ-irradiation (as a representative example) may be assessed using SEM. Figure 2(a) depicts a thick microstructure with indeterminate forms and almost uniform distribution, as well as an accumulation of partially overlapping or merged grains (a).

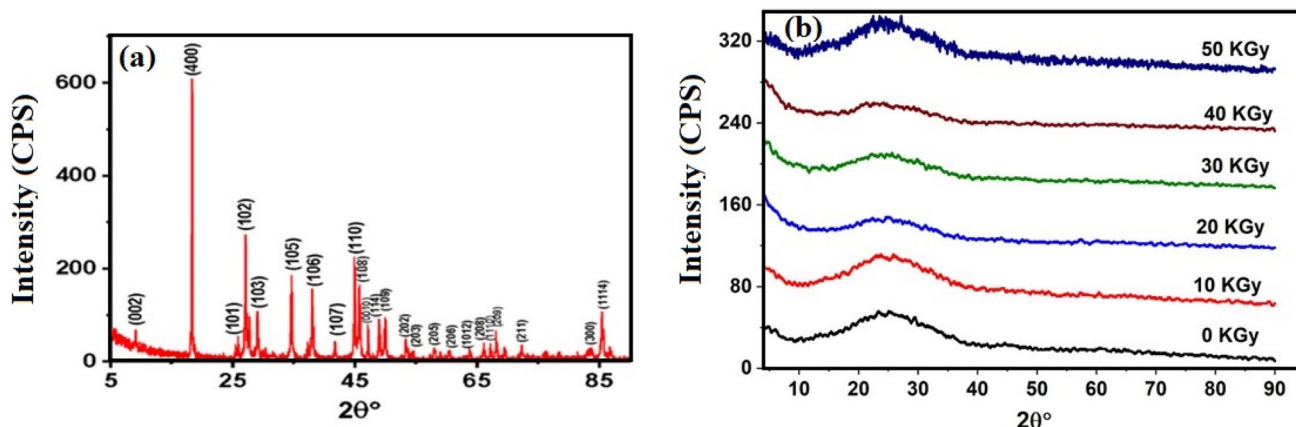


Fig. 1 a X-ray diffraction pattern of powder and b X-ray diffraction of pristine and γ -irradiated thin film of In_2Se_3

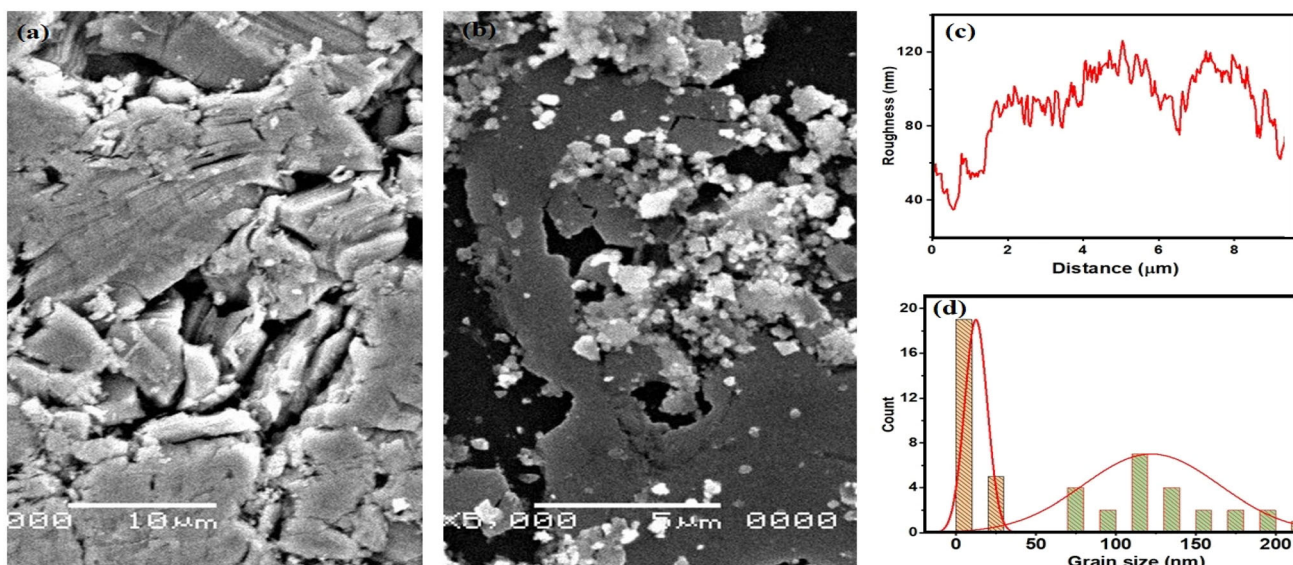


Fig. 2 SEM micrographs of In_2Se_3 a pristine film, b Irradiated thin films of 40 kGy gamma dose, c roughness of irradiated film, and d Grain size distribution of irradiated thin film of 40 kGy gamma dose

As a result of the γ -irradiation, irregular flattened forms were discovered, as shown in Fig. 2(b). Furthermore, by increasing the γ -irradiation dosage from 10 to 50 kGy, the diameters of these flattened forms were reduced, and a highly random grain distribution throughout the whole surface was increased (not shown here). The roughness is also estimated using the line profile distribution given in Fig. 2(c) and found to be in the 10–20 nm range. Consequently, the average grain size is predicted to be around 20 nm in the first range and 110 nm in the second range based on the histogram of the grain size distribution shown in Fig. 2(d). The grain size achieved is more than 20–120 nm due to the sample's aggregation

properties. The nanoparticle element is confirmed by SEM examination.

3.2 Optical characterization

For the prepared and irradiated surfaces, typical visual and near-infrared transmittance, $T(\lambda)$, and reflectance, $R(\lambda)$, in the range (10–50 kGy) for In_2Se_3 thin films are shown in Fig. 3(a, b). The transmittance and reflectance curves are consistently changed by γ -irradiation, as shown in these figures. In the absorption range (300–750 nm), the transmittance spectra of the irradiation films are moved to longer wavelengths (redshift) and have lower transmittance than the as-deposited film. Changes in the optical gap of

irradiated films cause these changes. While in the transparent area ($750 \text{ nm} < \lambda < 2500 \text{ nm}$), the as-deposited film exhibits greater transparency than the pristine films (96%) than the irradiated film (89%) with dose of 50 kGy. These modifications in optical transmission and reflectance of In_2Se_3 thin films may be associated to structural modification that is induced by influence of γ -irradiation. Figure 4(a) shows the spectrum behavior of the real, $n(\lambda)$ and imaginary parts of the indices, $k(\lambda)$ (not shown here) of pristine and γ -irradiated In_2Se_3 thin films. Moreover, Fig. 4(b, c) shows the influence of γ -irradiation on the values of n and k of In_2Se_3 thin film which decreases with the increase of dose values. The polarizability of the structure might explain the significant variation in the values n and k [18].

The spectrum behavior of the absorption coefficient, α for the as-deposited and γ -irradiated In_2Se_3 thin films is shown in Fig. 5. The intensity and absorption edge of In_2Se_3 are significantly changed when the γ -irradiation dose is raised.

The following equation was used to identify the type of electron transition and the value of the optical energy gap by examining the absorption coefficient around the onset and fundamental absorbing edge[19]:

$$(\alpha h\nu) = \beta(h\nu - E_g)^r, \tag{6}$$

where E_g is the optical energy gap, β is a constant, and r is a constant related to the type of transition (i.e., $r = 2$ and $1/2$ for indirect and direct permitted electronic transitions, respectively).

$r = 2$ and $1/2$ for indirectly and directly allowed electronic transitions, respectively, E_g is the optical energy gap, and β is the constant related to electronic conductivity. The type of electronic transition that is allowed is a direct transition that is determined by the best fit of data plot of $(\alpha h\nu)^2$ versus $(h\nu)$. Figure 6(a, b) depicts the variation between $(\alpha h\nu)^2$ vs. $(h\nu)$ for the pristine and γ -irradiated In_2Se_3 thin films, respectively. The extrapolated linear regression of the curve obtained from a plot of $(\alpha h\nu)^2$ vs. $(h\nu)$ is used to determine the direct band gap. The values of the optical gap for the as-deposited and γ -irradiated films are obtained by extrapolating the straight-line graphs $(\alpha h\nu)^2 = 0$.

The extrapolated linear regression of the curve obtained from a plot of $(h\nu)^2$ versus photon energy $(h\nu)$ is used to determine the direct band gap. The values of the optical gap for the as-deposited and γ -irradiated films are obtained by extrapolating the straight-line graphs $(\alpha h\nu)^2 = 0$. Figure 6 shows the change of the energy gaps of the pristine and the γ -irradiation that indicated a shift in the fundamental band gap energy from 2.48 to 1.67 eV, which is beneficial for solar cells. The degree of crystallinity effect in the In_2Se_3 thin films after exposure to γ -irradiation might explain the reduction in optical band gap. As a result of the increased disorder in the amorphous material caused by γ -irradiation, changes in the optical characteristics of the thin film occur. The computed energy gap values for the as-deposited thin films and irradiated with various γ -ray dose films with various doses are listed in Table 1. The findings show that optical energy gaps are affected

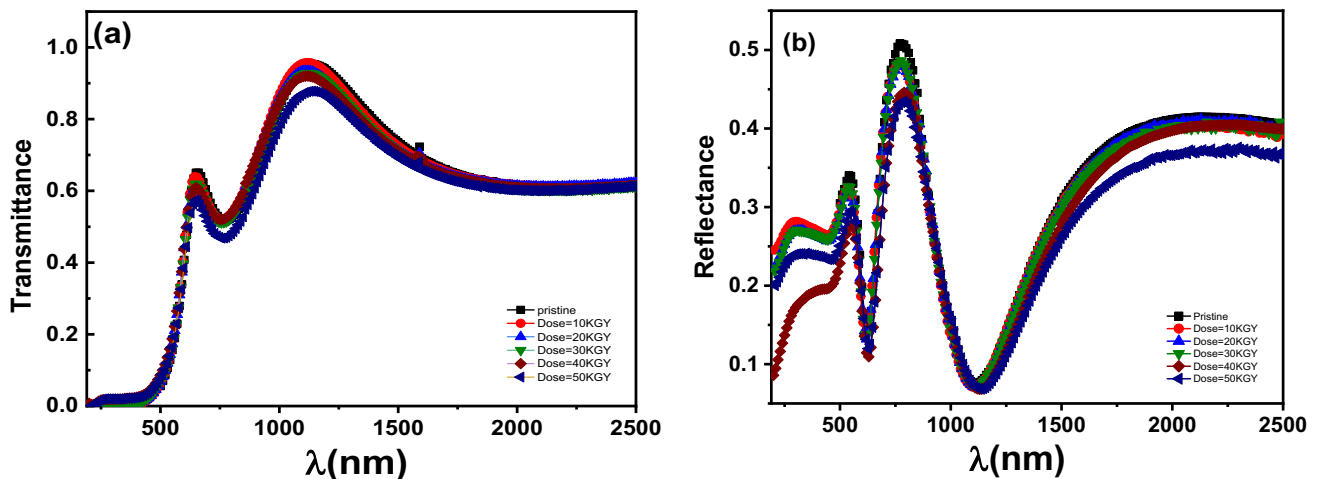


Fig. 3 Plot of the influence of γ -ray irradiation on the spectral distribution of a $T(\lambda)$, and b $R(\lambda)$ for pristine In_2Se_3 thin film

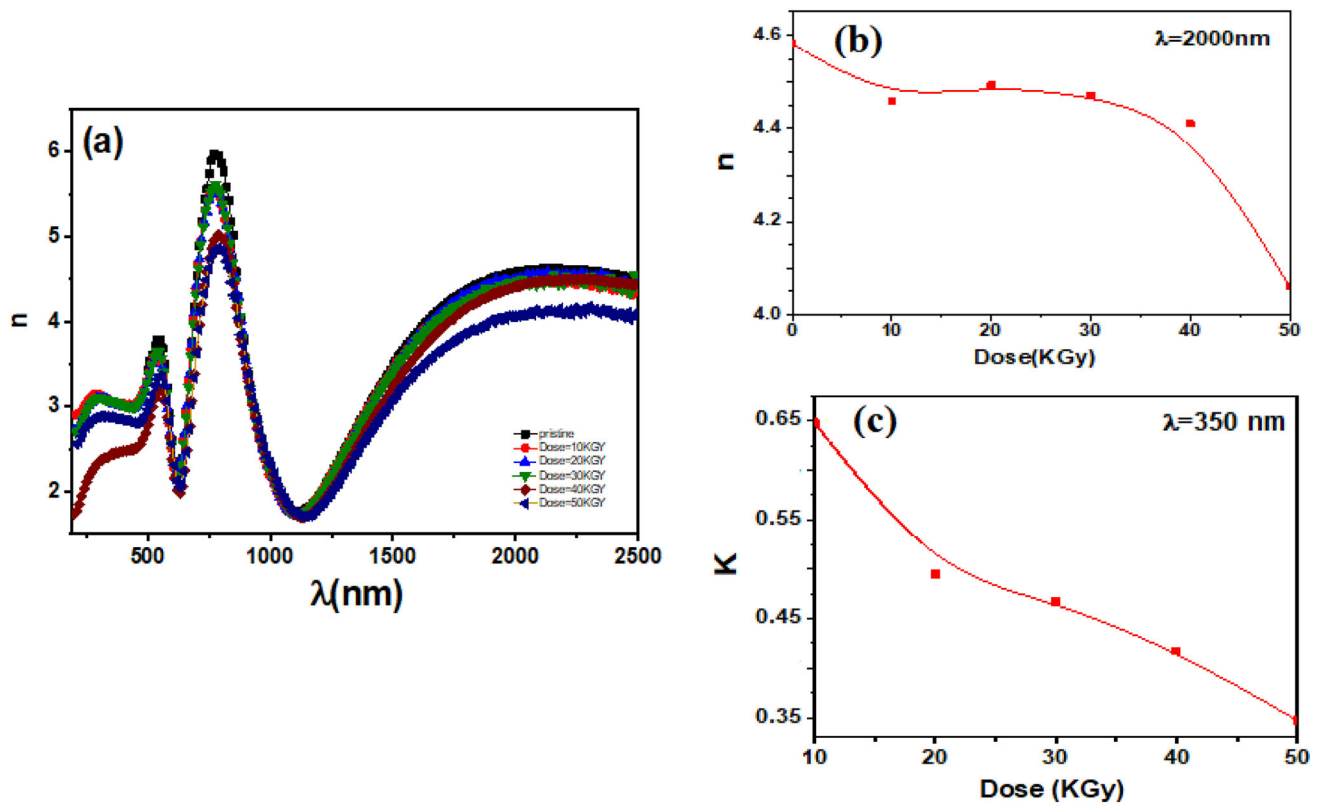


Fig. 4 Plot of the spectral behavior of the real, **a** $n(\lambda)$, and **b** Effect of doses on refractive index, and **c** Effect of doses on absorption coefficient k

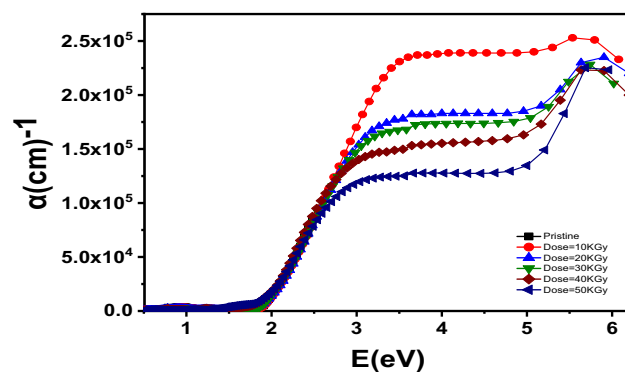


Fig. 5 The plots of α versus E for In_2Se_3 thin films before and after γ -irradiation

by the dosage of γ -irradiation. Furthermore, the fluctuation in the optical gap may be explained in terms of the increasing disorder and number of deformities in the structural bonding and crystal field induced by the structural flaws of gamma interaction with the thin films investigated [20]. The optical band gap reduces with more radiation doses, and this alteration has been related to the introduction of newly found electronic levels within the energy band

gap and the reduction because of structural rearrangements. This new energy level might be an acceptor near the valence band's apex or a donor lower in the conduction band, lowering the energy required to transfer the charge carrier from the valence band to the conduction band as discussed by Maity and Sharma [21]. Sharma [5] discovered that when gamma radiation dose increases, the optical band gap of tellurium dioxide thin films decreases. Aziz [22] discovered that exposing CdO thin films to radiation doses improves their behavior, as the values of optical characteristics rise with increasing radiation dosage owing to extra generation of energy levels inside the designated space between the equivalency and conduction band. Refaei et al. [23] found that the E_g values of CdSe thin films before irradiation (1.74) eV and the energy gap increased after irradiation; the rise in the gap is thought to be attributable to the rise in particle sizes. Stojilovic et al. [24] have found that radiation affects the optical properties resulting in a reduction of the optical band gap of the irradiated polymers. Obasi et al. [25] discovered that when the wavelength is increased, the

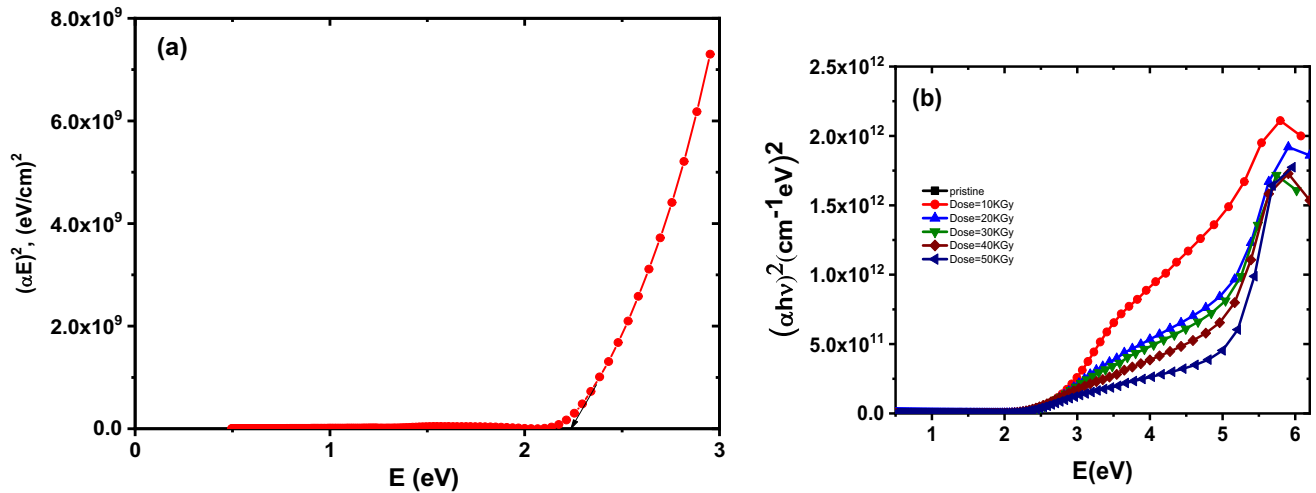


Fig. 6 Plot of the variation between E^2 versus $(h\nu)$ for the pristine and γ -irradiated In_2Se_3 thin films

Table 1 The optical gap and dispersion parameters In_2Se_3 for the pristine and γ -irradiated thin films

Film condition	E_g (eV)	E_u (eV)	E_d (eV)	E_o (eV)	ϵ_∞	N/m^* (10^{57}) m^{-3}/kg
Pristine	2.25	0.32	24.65	1.47	10.17	4.8
10 kGy	2.22	0.31	31.1	1.79	10.06	2.16
20 kGy	4.11	0.29	21.03	1.31	9.96	7.1
30 kGy	1.97	0.31	18.66	1.23	9.90	6.65
40 kGy	1.82	0.29	33.72	1.32	7.24	8.2
50 kGy	1.67	0.26	29.24	1.716	8.85	7.15

transmittance increases while the absorption coefficient falls, and as a result, the energy band gap of the sample reduces.

The Urbach energy may also be determined from the low-energy tail of the absorption coefficient. The linear response of the natural logarithm of absorption coefficient on photon energy is shown in Fig. 7(a). The Urbach energy is calculated by taking the inverse of the slope, as shown in Table 1 and Fig. 7(b) for varied γ -irradiation effect on the values of E_u . A decrease in the value of the Urbach energy was observed with an increase in the irradiation dose that is consistent with the change in the value of the gap energy explained above.

Furthermore, the refractive index values of In_2Se_3 show abnormal dispersion in the region 650 nm and normal dispersion in the range > 650 nm. Before and after γ -irradiation, the dispersion spectra in the transparent region (> 650 nm) were studied using the single-oscillator model given by Wemple and DiDomenico [26] as follows:

$$\frac{1}{n^2 - 1} = \frac{E_o}{E_d} - \frac{1}{E_o E_d} (h\nu)^2, \tag{7}$$

where E_o is the oscillator energy and E_d is the oscillator strength or dispersion energy. Figure 8(a) shows the plot of $(n^2 - 1)^{-1}$ versus $(h\nu)^2$ for the pristine and irradiated In_2Se_3 thin films. The slope and intercept on the vertical axis were used to get the values of E_o and E_d . Table 1 summarizes the E_o and E_d of the pristine and irradiated In_2Se_3 thin films and are illustrated in Fig. 9(a). The higher values of both E_o and E_d were observed for the dose of 10 kGy while it reaches to its lower values for the dose of 30 kGy. These findings indicate that γ -irradiation induces material structure.

For the dosage of 10 kGy, larger levels of E_o and E_d were obtained, whereas for the dose of 30 kGy, lower values were obtained. This change suggests that γ -irradiation causes material disorder that increases with increasing the dose value.

Furthermore, the refractive index can be resolved to get the high frequency dielectric constant (ϵ_∞). In the region of applied normal dispersion, the relationship between the actual dielectric constant and the wavelength is as follows [27]:

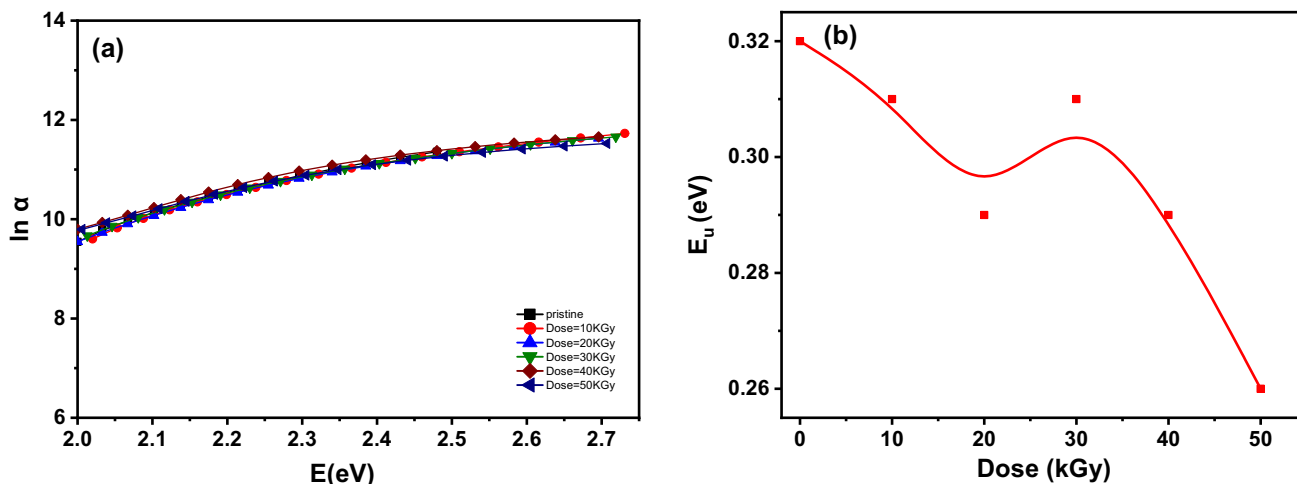


Fig. 7 a Plot of $\ln(\alpha)$ Vs. E at various doses, and b Urbach energy, E_u vs. Dose for In_2Se_3 thin films before and after γ -irradiation

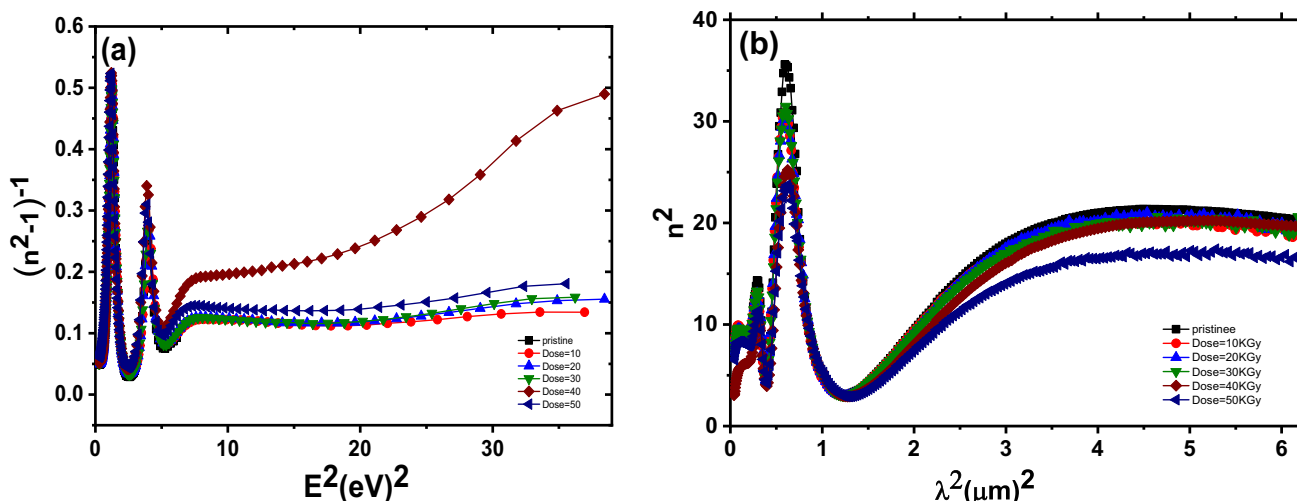


Fig. 8 The plots of a n^2 vs. λ^2 , and b $(n^2 - 1)^{-1}$ versus $(E)^2$ for the pristine and irradiated In_2Se_3 thin films

$$n^2 = \epsilon_L - \left[\left(\frac{e^2}{4\pi^2 \epsilon_0 c^2} \right) \left(\frac{N}{m^*} \right) \right] \lambda^2, \tag{8}$$

where ϵ_L and ϵ_0 are the lattice dielectric constant and the permittivity of free space, respectively. N/m^* is the ratio of free carrier concentration to its effective mass.

The change of n^2 for pristine and γ -irradiated In_2Se_3 thin films is shown in Fig. 8(b). In Table 1, the computed values of ϵ_∞ and N/m^* and are presented. After γ -irradiation treatment, the ϵ_∞ increases with the increase in the dose, as well as N/m^* values, but decreases at the dose of 40 kGy and then increases as shown in Fig. 9(b).

The frequency dispersal of complex dielectrics offers information on the material's electronic

structure, and the dielectric characteristics are associated with the crystals' electro-optic properties, making it crucial for the design of highly efficient optoelectronic devices. The acquired refractive and absorption indices allowed the real and imaginary parts of the complex dielectric constant to be calculated using the following relationships [28, 29]:

$$VELF = \frac{\epsilon_2}{\epsilon + i\epsilon_2} \tag{9}$$

$$\epsilon_1 = n^2 - k^2 \tag{10}$$

$$\epsilon_2 = 2nk \tag{11}$$

Figure 10(a, b) depicts the spectrum of real, ϵ_1 , and imaginary, ϵ_2 , components of the dielectric constant. As can be seen in this figure, the ϵ_1 has a higher value

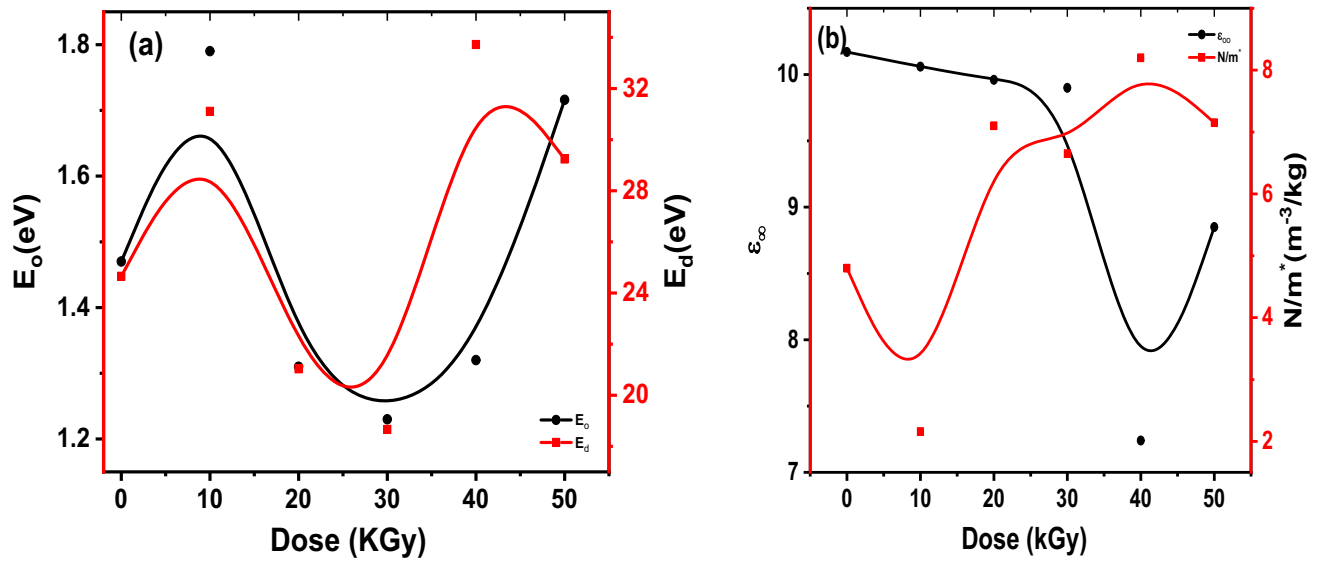


Fig. 9 a Plot of E_o and E_d vs. dose, and b Plot of ϵ_∞ and N/m^* vs. dose for In_2Se_3 thin film of various irradiation doses

than the value of ϵ_1 . Moreover, the dielectric constant, ϵ_1 displays a considerable rise at low energies and peaks at roughly 1.5 eV, and this peak moves toward increase as the irradiation value of the samples increases (blue shift). While ϵ_2 has a distinct pattern, with a sharp reduction at low energies and a broadening rise at around 3.2 eV. This rise is moved to higher energy by increasing the irradiation dosage, and then the values of ϵ_2 decrease. The effect of increasing photon energy on dielectric functions was also investigated. Figure 11(a, b) depicts the change in the value of the ϵ_1 at photon energies of 2.31 eV, as well as the change in the value of ϵ_2 at 2.31 eV. It is obvious that the highest values of both, ϵ_1 and ϵ_2 occur for the pristine films and that the values fall irregularly as the dose irradiation value increases.

The volume, VELF and surface energy loss functions, VELF and SELF, are linked to the real and imaginary portions of the dielectric constant by the following relationships [30]:

$$VELF = \frac{\epsilon_2}{\epsilon_1^2 + \epsilon_2^2} \tag{12}$$

$$SELF = \frac{\epsilon_2}{[(\epsilon_1 + 1)^2 + \epsilon_2^2]} \tag{13}$$

The distribution of volume (VELF) and surface (SELF) energy loss of the as-deposited and irradiated films as a function of photon energy is shown in Fig. 12(a, b). It is worth noting that the VELF value is larger than the SELF value, indicating that the energy loss inside is greater than the film's surface. Furthermore, for a given photon energy, the values of

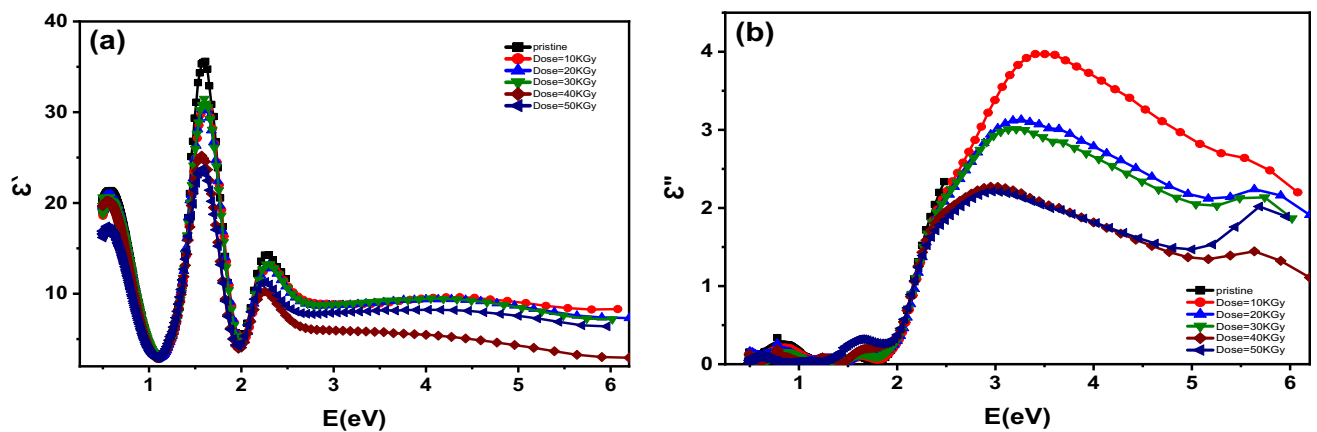


Fig. 10 a Plot of ϵ_1 vs. E , and b ϵ_2 vs. E for In_2Se_3 thin film of various irradiation doses

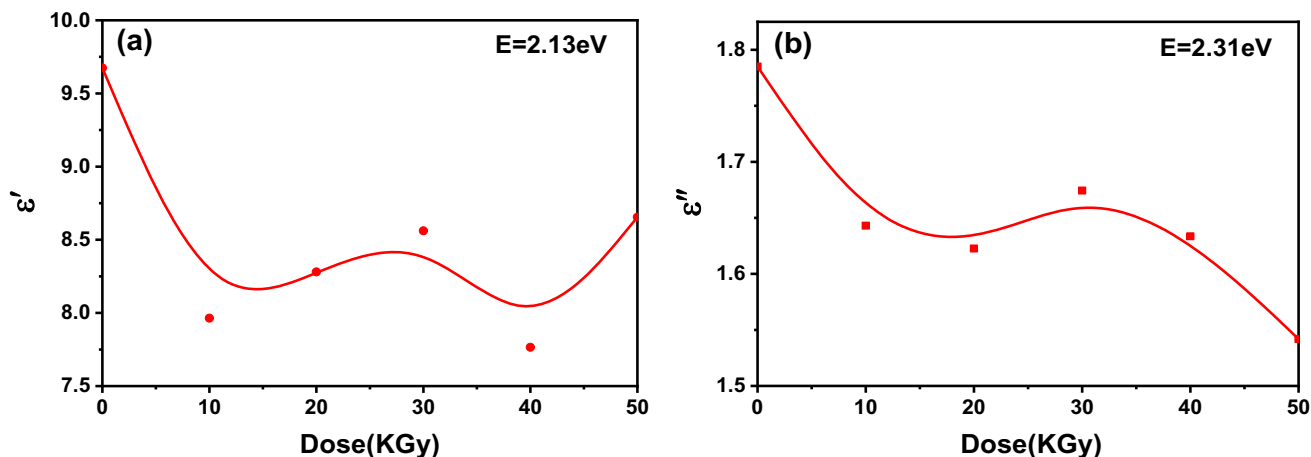


Fig. 11 **a** Plot of ε_1 vs. dose, and **b** Plot of ε_2 vs. dose for In_2Se_3 thin film of various irradiation doses

each VELF and SELF rise erratically, resulting in wide peaks at doses of 40 kGy (Fig. 13).

4 Nonlinear optical investigations

It is well known that the interaction of low-intensity radiation, such as conventional light, with the material is a linear function that creates linear optical results, but the interaction of high-intensity radiation, such as laser, is a nonlinear function that produces nonlinear optical results. The interaction of the induced polarization with the electric field utilized might cause the latter. The linear function can be achieved under influence of low-intensity field, but the nonlinear feature can be proven when for high field density [31].

The linear optical susceptibility of a material is calculated using the following relationship[31]:

$$\chi^{(1)} = \frac{(n^2 - 1)}{4\pi}. \quad (14)$$

However, the third nonlinear order susceptibility $\chi^{(3)}$, a key concept in a number of applications, depending on both the linear refractive index, n and $\chi^{(1)}$ can be represented as follows:[31]

$$\chi^{(3)} = A(\chi^{(1)})^4 = \frac{A}{(4\pi)^2}(n^2 - 1)^4, \quad (15)$$

where A is a constant of 1.7×10^{-10} esu, and $\chi^{(3)}$ denotes the limit of $h\nu \rightarrow 0$ ($n = n_0$).

Figure 14 (a, b) demonstrates the photon energy dependence of $\chi^{(1)}$ and $\chi^{(3)}$, respectively. Clearly, the two parameters have a peak at lower photon energy and saturate at greater photon energy to lower

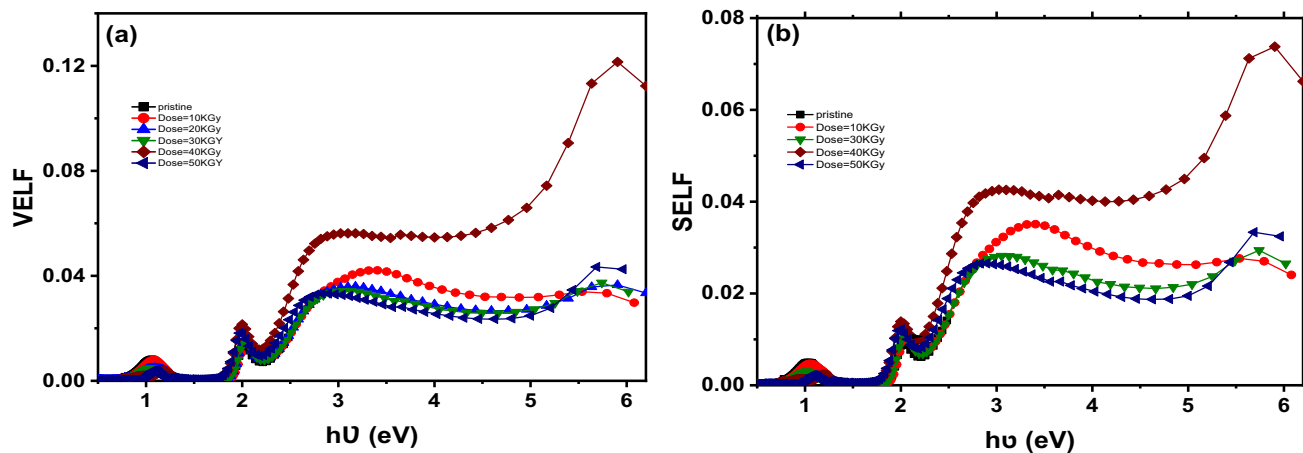


Fig. 12 **a** Plot of VELF vs. photon energy, $h\nu$ and **b** Plot of SELF vs. photon energy, $h\nu$ for the pristine and γ -irradiated In_2Se_3 thin films

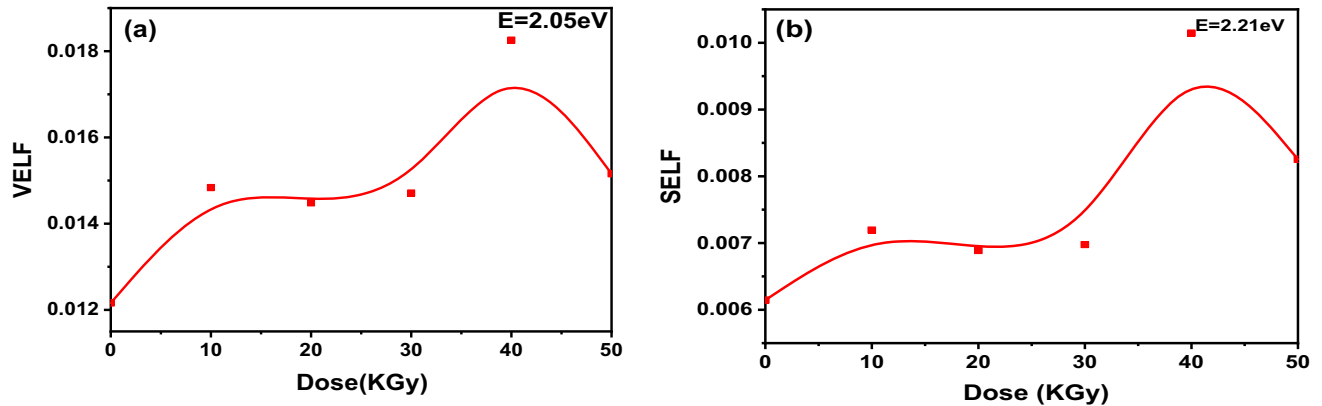


Fig. 13 a Plot of VELF vs. Dose, and b plot of SELF vs. Dose for the pristine and γ -irradiated In_2Se_3 thin films

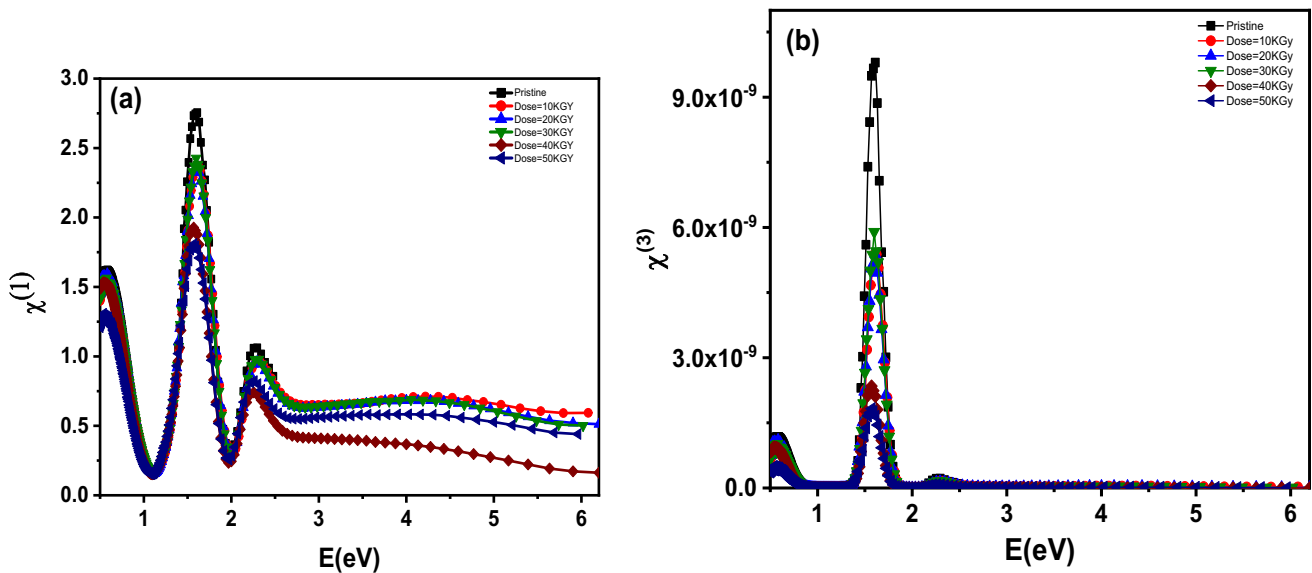


Fig. 14 a plot of $\chi^{(1)}$ vs. photon energy, hv and b Plot of $\chi^{(3)}$ vs. photon energy, hv for the pristine and γ -irradiated In_2Se_3 thin films

values. This high photon energy dependency is more easily understood for nonlinear optics applications. Clearly, the two parameters have a peak at lower photon energy and saturate at greater photon energy to lower values. This high photon energy dependency is more easily understood for nonlinear optics applications. The values of $\chi^{(3)}$ diminish when the irradiation dosage is increased as shown in Fig. 15 (a, b). The reduction in third-order nonlinear features for the samples tested may be attributed to a decrease in nonlinear refractive index. Because molecules with low $\chi^{(3)}$ have a large loss owing to two-photon absorption, they are suitable candidates for all optical switching applications[31].

5 Conclusion

The thermal evaporation process produces nanostructured In_2Se_3 films. Thin films of In_2Se_3 are sensitive to γ -irradiation of 10–50 kGy, indicating that they might be used in a variety of medical applications. According to the absorption study, the In_2Se_3 films as deposited and irradiated exhibit a direct permitted band gap. The Urbach energy was computed and is shown to be sensitive to the impact of irradiation doses, and the dependency of energy band gaps on irradiation dosage may be related to an increase in structural disorder when the dose is increased. This investigation was successful since it was able to

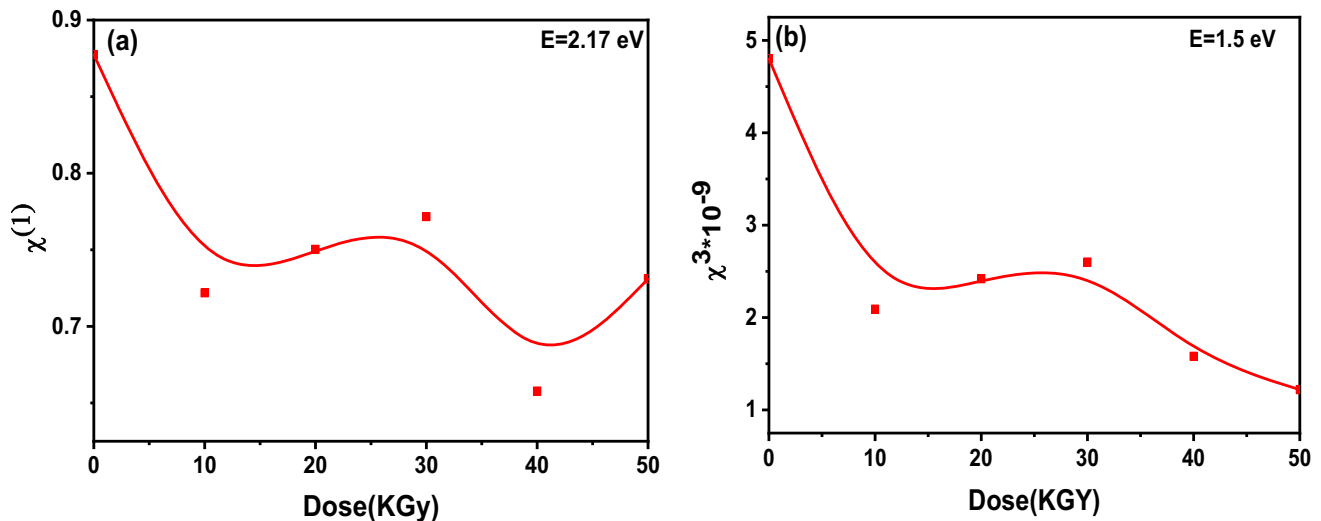


Fig. 15 a Plot of $\chi^{(1)}$ vs. Dose, and b plot of $\chi^{(3)}$ vs. Dose for the pristine and γ -irradiated In₂Se₃ thin films

extract and demonstrate how irradiation had an effect on the linear and nonlinear optical properties.

Acknowledgements

The authors would like to express their gratitude to the Physics Department, Faculty of Education, Ain Shams University as well as the Electronics Materials Dep. Advanced Technology & New Materials Research Inst., City of Science Research & Technological Applications (SRTA-City), for their contributions to the scientific findings.

Author contributions

BE: preparing the samples, X-ray measurement, optical spectroscopic measurement, Formal analysis of X-ray and optical properties, Writing—original draft, and final revision of the manuscript plagiarism. AAMF: Final analysis of SEM, and Final revision of all the figures and the manuscript writing and manuscript plagiarism. AHA: irradiated Samples and X-ray measurement. MME-N: preparing the Samples, and final revision of the manuscript. NR: Scanning electron microscope (SEM) measurements.

Funding

Open access funding provided by The Science, Technology & Innovation Funding Authority (STDF)

in cooperation with The Egyptian Knowledge Bank (EKB). The authors have not disclosed any funding.

Data availability

Data will be made available on responsible request.

Declarations

Conflict of interest The authors declare that they have no known competing financial interests or personal relationships that could have appeared to influence the work reported in this paper.

Open Access This article is licensed under a Creative Commons Attribution 4.0 International License, which permits use, sharing, adaptation, distribution and reproduction in any medium or format, as long as you give appropriate credit to the original author(s) and the source, provide a link to the Creative Commons licence, and indicate if changes were made. The images or other third party material in this article are included in the article's Creative Commons licence, unless indicated otherwise in a credit line to the material. If material is not included in the article's Creative Commons licence and your intended use is not permitted by statutory regulation or exceeds the permitted use, you will need to obtain permission directly from the copyright holder. To view a copy of this licence, visit <http://creativecommons.org/licenses/by/4.0/>.

References

- K. Lai, H. Peng, W. Kundhikanjana et al., Nanoscale electronic inhomogeneity in In_2Se_3 nanoribbons revealed by microwave impedance microscopy. *Nano Lett.* **9**, 1265–1269 (2009). <https://doi.org/10.1021/nl900222j>
- Z.D. Kovalyuk, V.M. Katerynychuk, A.I. Savchuk, O.M. Sydor, Intrinsic conductive oxide-p-InSe solar cells. *Mater. Sci. Eng. B* **109**, 252–255 (2004). <https://doi.org/10.1016/j.mseb.2003.10.074>
- K. Yilmaz, M. Parlak, and C. Ercelebi, Investigation of photovoltaic properties of amorphous InSe thin film based Schottky devices. *Semicond. Sci. Technol.* **22**, 1268–1271 (2007). <https://doi.org/10.1088/0268-1242/22/12/004>
- S. Koliopoulou, P. Dimitrakis, D. Goustouridis, P. Normand, C. Pearson, M.C. Petty, H. Radamson, D. Tsoukalas, Metal nano-floating gate memory devices fabricated at low temperature. *Microelectron. Eng.* **83**, 1563–156 (2006). <https://doi.org/10.1016/j.mee.2006.01.235>
- C.H. De Groot, J.S. Mooodera, Growth and characterization of a novel In_2Se_3 structure. *J. Appl. Phys.* **89**, 4336–4340 (2011). <https://doi.org/10.1155/2011/976262>
- M. Emziane, R. Le Ny, “Crystallization of In_2Se_3 semiconductor thin films by post-deposition heat treatment. thickness and substrate effects. *J. Phys. D* **32**, 1319–1328 (1999). <https://doi.org/10.1088/0022-3727/32/12/307>
- A.A. Homs, B. Mari, Photoluminescence of undoped and neutron-transmutation-doped InSe. *J. Appl. Phys.* **88**, 4654–4659 (2000). <https://doi.org/10.1063/1.1308066>
- B. Gurbulak, Urbach tail and optical investigations of Gd doped and undoped InSe single crystals. *Physica Scripta* **70**, 197–201 (2004). <https://doi.org/10.1088/0031-8949/70/2-3/020>
- I.H. Choi, P.Y. Yu, Properties of phase-pure InSe films prepared by metalorganic chemical vapor deposition with a single-source precursor. *J. Appl. Phys.* **93**, 4673–4677 (2003). <https://doi.org/10.1063/1.1561584>
- Du. Yong, Xu. Buqing, Guilei Wang, Yuanhao Miao, Ben Li, Zhenzhen Kong, Yan Dong, Wenwu Wang, Henry H. Radamson, Review of highly mismatched III-V heteroepitaxy growth on (001) silicon. *Nanomaterials* **12**, 741–787 (2022). <https://doi.org/10.3390/nano12050741>
- H. Zeyada, M. Makhlof, M. El-Nahass, Influence of gamma ray irradiation and annealing temperature on the optical constants and spectral dispersion parameters of metal-free and zinc tetraphenylporphyrin thin films: a comparative study. *Spectrochim. Acta A* **148**, 338–347 (2015). <https://doi.org/10.1016/j.saa.2015.04.008>
- S. Ahmad, S. Islam, M. Nasir, K. Asokan, M. Zulfequar, Effects of gamma-ray irradiation on the optical properties of amorphous $\text{Se}_{100-x}\text{Hg}_x$ thin films. *J. Phys. Chem. Solids* **117**, 122–130 (2018). <https://doi.org/10.1016/j.jpcs.2018.02.014>
- M.M. El-Nahass, Optical properties of tin diselenide films. *J. Mater. Sci.* **27**, 6597–6604 (1992). <https://doi.org/10.1007/BF01165942>
- H.M. Zeyada, M.M. Makhlof, M.A. Ali, Structural, optical and dispersion properties of 5, 10, 15, 20-tetraphenyl-21H, 23H-porphyrin zinc thin films. *Jpn. J. Appl. Phys.* **55**, 022601 (2016). <https://doi.org/10.7567/JJAP.55.022601>
- Ji Pankove 2012 Optical Processes in Semiconductors, Courier Corporation
- M. El-Nahass, H. Soliman, N.E. Kadry, A. Morsy, S. Yagmour, A new computational method for determining the optical constants and its application for CuInS_2 thin films. *J. Mater. Sci. Lett.* **7**, 1050–1053 (1988). <https://doi.org/10.1007/BF00720823>
- R. Shirley, The CRYSFIRE system for automatic powder indexing: user’s manual. *The Lattice Press* **41**, 931–932 (2000)
- S. Ahmad, K. Asokan, M. Shahid Khan, M. Zulfequar, Effect of ^{60}Co γ -irradiation on structural and optical properties of thin films of $\text{Ga}_{10}\text{Se}_{80}\text{Hg}_{10}$. *Philos. Mag.* **95**, 2385–2402 (2015). <https://doi.org/10.1080/14786435.2015.1059518>
- J. Bardeen, F. Blatt, L. Hall, *Photoconductivity Conference*, vol. 195623 (Wiley, New York, 1956), p.146
- S.M. El-Sayed, Electron beam and gamma irradiation effects on amorphous chalcogenide $\text{SbSe}_{2.5}$ film. *Nucl. Instrum. Methods Phys. Res. B* **225**, 535 (2004)
- TK Maity SL Sharma 2011 Effects of gamma irradiation on the electrical, optical and structural properties of tellurium dioxide thin films *Indian J. of Pure App. Phys.* 606-612
- A.A. Aziz, The effect of exposure to alpha particles on the optical properties of the CdO thin film. *J. Sc. Al-Nahrain Univ.* **15**(2012), 27–31 (2012)
- D.H. Al Refaei, L.M. Al Taan, L.A. Najam, The effect of α -particles on structural, optical and morphological properties for cadmium selenide thin film. *J. Phys.* **1973**, 012155 (2021). <https://doi.org/10.1088/1742-6596/1973/1/012155>
- N. Stojilovic, S.V. Dordevic, S. Stojadinovic, Effects of clinical X-ray irradiation on UHMWPE films. *Nucl. Instrum. Methods Phys. Res. B* **410**, 139–143 (2017). <https://doi.org/10.1016/j.nimb.2017.08.023>
- C.O. Obasi, I.L. Ikhioya, A.S. Ahmad, A.M. Ramalan, Effect of Gamma radiation (^{60}Co) on the optical transmittance, energy gap and absorption coefficient of ZnSe thin films. *Inter. J. Eng. Appl Sci. Technol.* **4**, 224–228 (2019)
- S. Wemple, M. DiDomenico Jr., Behavior of the electronic dielectric constant in covalent and ionic materials. *Phys. Rev. B* **3**, 1338 (1971). <https://doi.org/10.1103/PhysRevB.3.1338>

27. P. Edward, *Handbook of Optical Constants of Solids* (Academic Press, New York, 1985)
28. M. Dongol, M.M. El-Nahass, A. El-Denglawey, A.F. Elhady, A.A. Abuelwafa, *Curr. Appl. Phys.* **12**, 1178 (2012). <https://doi.org/10.1016/j.cap.2012.02.051>
29. M.M. El-Nahass, A.M. Hassanien, F.S.H. Abu-Samaha, Eman Elesh. *Opt. Commun.* **325**, 1 (2014). <https://doi.org/10.1016/j.optcom.2014.03.077>
30. R.J. Bell, M.A. Ordal, R.W. Alexander, Equations linking different sets of optical properties for nonmagnetic materials. *J. Appl. Opt.* **24**, 3680 (1985). <https://doi.org/10.1364/AO.24.003680>
31. B. Shanmugavelu, V.R.K. Kumar, R. Kuladeep, D.N. Rao, Third order nonlinear optical properties of bismuth zinc borate glasses. *J. Appl. Phys.* **114**, 243103 (2013). <https://doi.org/10.1063/1.4858422>

Publisher's Note Springer Nature remains neutral with regard to jurisdictional claims in published maps and institutional affiliations.